

Supporting Information

Guanidinium solvents with exceptional hydrogen bond donating abilities

Navneet K. Brar, Roland T. Brown, Kaveh Shahbaz, Patricia A. Hunt and Cameron C. Weber

Table of Contents

Methods	2
General Procedures.....	2
Synthesis of DESs.....	2
Kamlet Taft Parameters	2
Pyridine N-Oxide Probe.....	3
Tributylphosphine Oxide Probe.....	3
Nile Red Probe	3
Computational Methods	3
Guanidinium Deep Eutectic Solvent Preparation.....	4
Polarity Parameter Calculations	6
Kamlet-Taft Parameters – Solvatochromic Dyes.....	6
Kamlet Taft Parameters – Pyridine N-Oxide.....	7
Development of Tributylphosphine Oxide Polarity Scale.....	8
Nile Red	11
Polarity Parameter Results.....	12
Kamlet-Taft Parameters.....	12
Nile Red Polarity Measurements	14
Density and Viscosity Measurements	16
Computational Details	17
References	24

Methods

General Procedures

2,6-dichloro-4-(2,4,6-triphenyl-N-pyridino)-phenolate (Reichardt's betadine dye 33), 4-nitroaniline, N,N-diethyl-4-nitroaniline, pyridine N-oxide, guanidinium chloride, DL-lactic acid, acetamide, levulinic acid, glycerol, oxalic acid, malic acid, succinic acid, urea, serine, decanoic acid, adipic acid, oxalic acid dihydrate, PEG400, citric acid, sorbitol, glucose, glycolic acid, 1-decanol, catechol, tributyl phosphine oxide, acetic acid, n-hexane, toluene hexafluoroisopropanol, trimethyl phosphate and Nile red were purchased from commercial suppliers and were used as received.

The following solvents were purified using an LC Technology Solutions Inc SP-1 solvent purification system: acetonitrile, 1,2-dichloroethane, dichloromethane, diethyl ether, dimethylformamide, methanol, tetrahydrofuran.

The ionic liquids (ILs) [C₄C₁im][OTf], [C₄C₁im][NTf₂] and [C₄C₁im][N(CN)₂] were prepared as described previously,^{1,2} with the exception that the halide content of [C₄C₁im][N(CN)₂] was assessed using a saturated AgN(CN)₂ solution. Ionic liquids were dried overnight under high vacuum at 50°C prior to use.

UV-vis absorption spectra were obtained using a Cary 300 UV-Visible spectrometer equipped with a water recirculating Peltier temperature controller. NMR spectra were obtained using a Bruker Avance 400 MHz spectrometer. Melting points were determined using a digital melting point apparatus (MPS20).

Density and viscosity measurements were performed using an integrated Anton Paar DMA 4100/Lovis 2000 ME module. Reported accuracies for this instrument are ±0.0001 g cm⁻³ for density and ±0.5% for viscosity.

Synthesis of DESs

DESs were prepared by directly weighing components in the desired mole ratio and then either stirring the mixture at elevated temperature (50-80°C for 1-2 h) or grinding the mixture at room temperature using a mortar and pestle until a homogenous mixture had been formed.

Kamlet Taft Parameters

Solutions containing 0.9 mM 4-nitroaniline and *N, N*-diethyl-4-nitroaniline and 0.4 mM of Reichardt's dye 33 were separately prepared in dichloromethane. An aliquot of this solution (100 µL for 4-nitroaniline and Reichardt's Dye 33, 35 µL for *N, N*-diethyl-4-nitroaniline) was

added to the cuvette and the dichloromethane evaporated. The precipitated dye was dissolved in the DES in the cuvette and the UV-vis absorption spectrum measured with the temperature controlled using a water recirculated Peltier temperature controller. The Kamlet Taft parameters α , β and π^* were calculated from the wavelength of the lowest energy absorption as described in the polarity parameter calculation section below. Polarity measurements were obtained at 25, 40, 60 and 80°C.

Pyridine N-Oxide Probe

Solutions of 0.25 M pyridine N-oxide (PyO) were prepared in each solvent with a flame-sealed, coaxially inserted capillary containing DMSO-d₆ used as an NMR lock.³ The ¹³C NMR of these samples was obtained and used to calculate the α Kamlet-Taft parameter as described in the polarity parameter calculation section below.^{3, 7} These measurements were obtained at 25, 40, 60 and 80°C.

Tributylphosphine Oxide Probe

Tributylphosphine oxide (TBPO) (0.010 g, 0.046 mmol) was separately dissolved in 0.75 mL of the desired solvent and a coaxially inserted, flame-sealed capillary containing 0.5 M trimethyl phosphate in DMSO-d₆ was used as an NMR lock and ³¹P internal standard (δ 3.5 ppm). These solutions were then analysed by ³¹P NMR with the chemical shift related to Kamlet Taft parameters as described in the polarity parameter calculation section.

Nile Red Probe

Nile red (13 mg, 0.042 mmol) was dissolved in 100 mL of acetone. 100 μ L aliquots of the acetone and Nile red solution were then added to a cuvette with the acetone evaporated under a flow of air. The precipitated Nile red was then dissolved in 1 mL of the desired solvent, with the UV-vis absorption spectra obtained at 25°C.

Computational Methods

A qualitative estimate of the Kamlet-Taft α has been obtained using an established methodology for ILs based on an empirical relationship between the computed electrostatic potential (EP_{nuc}) at the most acidic H-atom (which is also the H-atom with the smallest EP_{nuc}), neglecting the charge on the H-atom itself.⁴ The IL based empirical formula employed is $\alpha_{\text{EP}} = 5.153 * EP_{\text{nuc}} + 5.136$. This empirical relationship was determined at the B3LYP/6-311+G(d,p) level, hence to enable the use of this relationship the calculations carried out here are also at the B3LYP/6-311+G(d,p) level.

Calculations are carried out using Gaussian 16 (Revision C.01)^a. For all calculations no symmetry constraints have been applied, the scf convergence of the RMS density matrix is 10^{-9} for the gas-phase and 10^{-11} for SMD calculations. All structures have been optimised, and confirmed as minima by the absence of imaginary frequencies. The changes in thermochemical Gibbs free energies have also been evaluated and are reported.

A generalised solvation environment employing the SMD model has been utilised.^{5, 6} SMD requires a range of input parameters for LA. We employed a static dielectric constant $\epsilon=5.0^7$ and refractive index $n^2=2.071$.⁸ We could find no report of the surface tension (γ) of lactic acid, and thus estimated γ based on similar liquids (at 25 °C in units of mN m^{-1}) including acetic acid (26.60), propanoic acid (26.20), butanoic acid (26.05) and 2-hydroxy butanoic acid (37.7).⁸ Since there is little variation for these acids, we took the value for 2-hydroxy butanoic acid as the most similar to lactic acid, thus $\gamma=37.7 \text{ mN m}^{-1} * 1.43932 = 54.3 \text{ cal mol}^{-1} \text{ \AA}^{-2}$. ϕ is the fraction of non-hydrogen atoms which are aromatic carbon atoms and ψ is the fraction of non-hydrogen atoms which are electronegative halogen atoms, both are zero for LA. The Abrahams acidity and basicity $\Sigma\alpha^{\text{H}}$ and $\Sigma\beta^{\text{H}}$ are derived from the experimental Kamlet-Taft α and β parameters reported within this work via a previously established empirical conversion formula.⁴

^a Gaussian 16, Revision C.01, M. J. Frisch, G. W. Trucks, H. B. Schlegel, G. E. Scuseria, M. A. Robb, J. R. Cheeseman, G. Scalmani, V. Barone, G. A. Petersson, H. Nakatsuji, X. Li, M. Caricato, A. V. Marenich, J. Bloino, B. G. Janesko, R. Gomperts, B. Mennucci, H. P. Hratchian, J. V. Ortiz, A. F. Izmaylov, J. L. Sonnenberg, D. Williams-Young, F. Ding, F. Lipparini, F. Egidi, J. Goings, B. Peng, A. Petrone, T. Henderson, D. Ranasinghe, V. G. Zakrzewski, J. Gao, N. Rega, G. Zheng, W. Liang, M. Hada, M. Ehara, K. Toyota, R. Fukuda, J. Hasegawa, M. Ishida, T. Nakajima, Y. Honda, O. Kitao, H. Nakai, T. Vreven, K. Throssell, J. A. Montgomery, Jr., J. E. Peralta, F. Ogliaro, M. J. Bearpark, J. J. Heyd, E. N. Brothers, K. N. Kudin, V. N. Staroverov, T. A. Keith, R. Kobayashi, J. Normand, K. Raghavachari, A. P. Rendell, J. C. Burant, S. S. Iyengar, J. Tomasi, M. Cossi, J. M. Millam, M. Klene, C. Adamo, R. Cammi, J. W. Ochterski, R. L. Martin, K. Morokuma, O. Farkas, J. B. Foresman, and D. J. Fox, Gaussian, Inc., Wallingford CT, 2019.

Guanidinium Deep Eutectic Solvent Preparation

20 combinations of hydrogen bond donors (HBDs) with guanidinium chloride were explored. The structures of all HBDs examined are depicted in Figure S1. The melting point of the mixtures was recorded where a solid mixture resulted. These results are provided in Table S1. Mixtures that remained liquid after cooling to room temperature are simply denoted “liquid”. It is evident from Table S1 that only 4 combinations yielded room temperature liquids although several did form eutectic mixtures, with some of the eutectic mixtures leading to significant decreases in melting points.

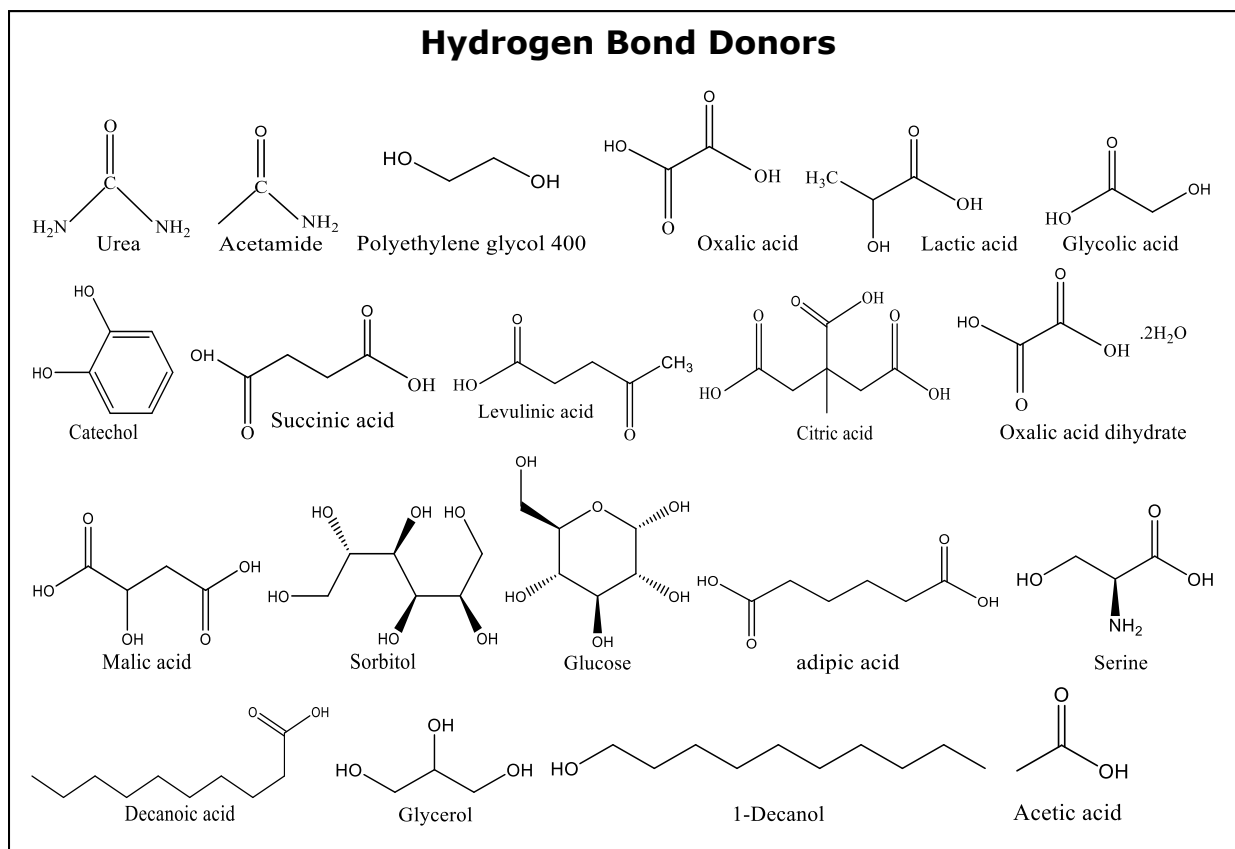


Figure S1. Structures of HBDs explored.

Table S1. Composition and melting point of lowest melting mixtures of GuCl and each HBD as determined using a melting point apparatus. HBD melting point is provided for reference. < 25°C indicates a room temperature liquid.

HBD	HBD m.p.	GuCl:HBD	GuCl:HBD m.p.
Oxalic acid dihydrate	101°C	1:1	46°C
Succinic acid	184°C	2:3	125°C
Acetamide	80°C	1:9	<25°C*
Glucose	150°C	1:1	68°C
Malic acid	129°C	1:1	57°C
Urea	134°C	3:7	72°C
Levulinic acid	34°C	1:9	<25°C
Glycolic acid	75°C	1:9	Not miscible
PEG 400	6°C	1:9	Not miscible
Oxalic acid anhydrous	190°C	3:7	160°C
Lactic acid	17°C	3:7	<25°C

Catechol	105°C	1:1	47°C
Decanoic acid	31°C	1:9	Not miscible
Acetic acid	17°C	1:9	Not miscible
Glycerol	19°C	3:7	<25°C
Sorbitol	95°C	1:1	<25°C**
Serine	237°C	1:1	149°C
1-decanol	6°C	1:9	Not miscible
Citric acid	156°C	3:7	98°C
Adipic acid	152°C	1:1	126°C
Glycolic acid	75°C	1:9	Not miscible

*Liquid found later to be metastable, ** Paste that solidified on standing

Polarity Parameter Calculations

Kamlet-Taft Parameters – Solvatochromic Dyes

The Kamlet-Taft parameters α , β and π^* are typically determined using a solvatochromic dye set. A commonly used dye set for the determination of these parameters for alternative solvents such as ionic liquids and DES involves Reichardt's Dye 30 or Reichardt's Dye 33, N,N-diethyl-4-nitroaniline and 4-nitroaniline (Figure S2).^{9, 10}

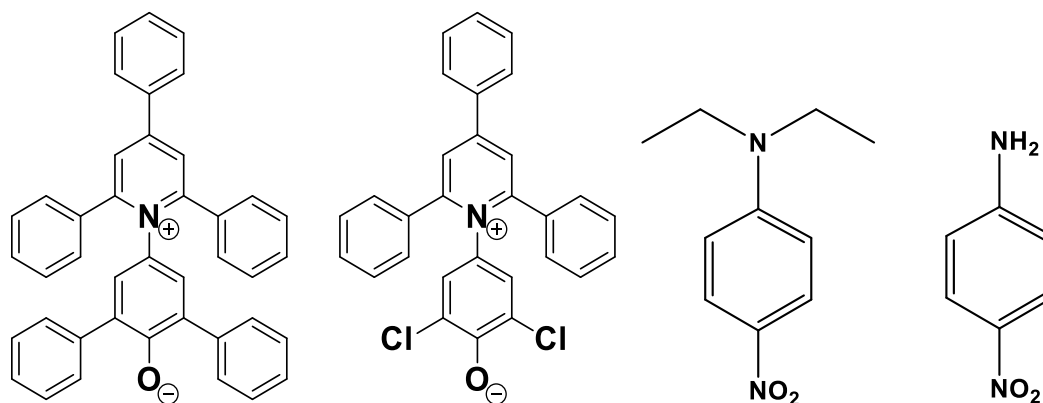


Figure S2. Solvatochromic dye molecules typically used to determine Kamlet-Taft parameters in ionic liquids and deep eutectic solvents. From left: Reichardt's Dye 30, Reichardt's Dye 33, N,N-diethyl-4-nitroaniline, 4-nitroaniline.

The Kamlet-Taft parameters can be calculated from this dye set using Equations S1-S3 below. $\bar{\nu}$ is the experimental wave number (cm^{-1}) of the lowest energy absorption maximum with D4NA standing for N,N-diethyl-4-nitroaniline and 4NA for 4-nitroaniline.¹⁰ $E_T(30)$ is

determined using Equation S4 based on the lowest energy absorption maximum of Reichardt's Dye 30 (in nm).

$$\pi^* = 0.314(27.52 - \bar{\nu}_{D4NA}) \quad (S1)$$

$$\alpha = 0.0649E_T(30) - 2.03 - 0.72\pi^* \quad (S2)$$

$$\beta = \frac{1.035\bar{\nu}_{D4NA} + 2.64 - \bar{\nu}_{4NA}}{2.80} \quad (S3)$$

$$E_T(30) = \frac{28591}{\lambda_{max}} \quad (S4)$$

Reichardt's Dye 33 is a less basic analogue of Reichardt's Dye 30 which makes it more compatible with acidic solvents. $E_T(33)$ values are computed using Equation S5 using the lowest energy absorption maximum for Reichardt's Dye 33, analogous to the calculation for $E_T(30)$. The empirical relationship between $E_T(30)$ and $E_T(33)$ that has been determined using linear regression is given by Equation S6,¹¹ facilitating the direct determination of α from $E_T(33)$ using Equation S7.

$$E_T(33) = \frac{28591}{\lambda_{max}} \quad (S5)$$

$$E_T(30) = 0.9953E_T(33) - 8.1132 \quad (S6)$$

$$\alpha = 0.0646E_T(33) - 2.56 - 0.72\pi^* \quad (S7)$$

Kamlet Taft Parameters – Pyridine N-Oxide

Despite the reduced acid-sensitivity of Reichardt's Dye 33, it was found that it was still bleached in the presence of carboxylic acid containing solvents. To overcome this problem, pyridine-N-oxide (Figure S3), was used as an alternative probe as it has been shown previously as a viable probe for the determination of α values.³ Unlike the solvatochromic dyes conventionally used, pyridine N-oxide uses the ¹³C chemical shift difference (ppm) between carbon 4 with either carbon 2 (d_{24}) or 3 (d_{34}) to enumerate the α value, denoted α_{24} and α_{34} . These values are calculated using Equations S8 and S9 respectively.

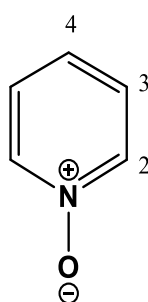


Figure S3. Structure of pyridine-N-oxide with ring positions numbered.

$$\alpha_{24} = 2.32 - 0.15 \times d_{24} \quad (\text{S8})$$

$$\alpha_{34} = 0.40 - 0.16 \times d_{34} \quad (\text{S9})$$

Empirical linear regression has been found that $\alpha_{24} = 0.88\alpha_{\text{RD}}$ where α_{RD} is the α value calculated using Equations S2 or S7.³ Hence dividing α_{24} by 0.88 should yield a comparable value of α to that obtained using Reichardt's Dye 30 or 33 as part of the dye set. In this paper we have denoted this value α_{PyO} , defined as per Equation S10. For our data we noticed that the α_{24} values appear to more accurately reproduce α_{RD} than the α_{PyO} values so α_{24} has been primarily used for comparison. Nonetheless, α_{PyO} values for all of the solvents explored are detailed in Table S10.

$$\alpha_{\text{PyO}} = \frac{\alpha_{24}}{0.88} \quad (\text{S10})$$

Development of Tributylphosphine Oxide Polarity Scale

Table S2 contains the ³¹P chemical shifts observed for tributylphosphine oxide with respect to the internal standard of 0.5 M trimethylphosphate in DMSO-d₆ (δ 3.5 ppm) alongside Kamlet-Taft parameters for the solvents used to calibrate and validate the ³¹P NMR scale. Hexane and dichloromethane values were performed in triplicate to examine the reproducibility of the procedure and both returned standard deviations of less than 0.1 ppm. The use of different TBPO concentrations for acetonitrile also had limited effect on the TBPO chemical shift with the chemical shift changing less than 0.5 ppm as the mass of TBPO was increased 50-fold from 2 mg to 100 mg and this change appearing to be random rather than systematic in nature.

Table S2. Kamlet-Taft parameters^{9, 12} and ³¹P NMR chemical shift of solvents used to calibrate and validate the ³¹P NMR scale for tributylphosphine oxide. Reported errors are standard deviations of triplicate experiments performed to verify the reproducibility of the procedure.

Solvent	α	β	π^*	δ ³¹ P (ppm)
Hexane	0.00	0.00	-0.04	40.54 ± 0.09
Diethyl ether	0.00	0.47	0.27	41.62
Toluene	0.00	0.11	0.54	42.08
Tetrahydrofuran	0.00	0.55	0.58	42.55
Dimethylformamide	0.00	0.69	0.88	45.92
1,2-Dichloroethane	0.00	0.10	0.81	46.58

Dimethylsulfoxide	0.00	0.76	1.00	47.17
Acetonitrile	0.19	0.40	0.75	47.58
Dichloromethane	0.13	0.10	0.82	47.73 ± 0.06
[C ₄ C ₁ im][OTf]	0.62	0.49	1.00	49.00
[C ₄ C ₁ im][NTf ₂]	0.72	0.23	0.99	49.69
[C ₄ C ₁ im][N(CN) ₂]	0.54	0.60	1.05	49.95
Methanol	0.98	0.66	0.60	57.00
Acetic acid	1.12	0.45	0.64	61.67
Water	1.17	0.47	1.09	62.12
HFIP	1.96	0.00	0.65	64.64
Acetonitrile ^a	-	-	-	47.19
Acetonitrile ^b	-	-	-	47.07
Aq. HCl ^c	-	-	-	62.59

^a0.002 g TBPO used (not used for calibration)

^b0.100 g TBPO used (not used for calibration)

^c2.5 mol eq. HCl relative to TBPO (not used for calibration)

To investigate the relationship between the ³¹P NMR chemical shifts obtained and the Kamlet-Taft parameters, multiple linear regressions were performed of the type outlined in Equation S11 below. When at least one parameter was found to be not significant at the 0.05 level of significance then a multiple linear regression with combinations of the remaining parameters was performed until a satisfactory fit was obtained. Tables S3-S9 summarise the outcomes of these linear regressions in terms of the value of each coefficient, the p-values obtained for each coefficient as well as the R² value. Note that R² values can only be meaningfully compared between models possessing the same number of parameters.

$$\delta_{TBPO} = a\alpha + b\beta + p\pi^* + c \quad (\text{S11})$$

Table S3. Coefficient and p-value of parameters obtained from multiple linear regression of δ_{TBPO} with inclusion of α , β and π^* .

	a	b	p	c
Coefficient	11.83	2.60	3.18	22.73

p-value	<0.0001	0.38	0.21	<0.0001
R²		0.907		

Table S4. Coefficient and p-value of parameters obtained from multiple linear regression of δ_{TBPO} with inclusion of α and β .

	a	b	c
Coefficient	12.28	4.22	42.43
p-value	<0.0001	0.12	<0.0001
R²		0.895	

Table S5. Coefficient and p-value of parameters obtained from multiple linear regression of δ_{TBPO} with inclusion of α and π^* .

	a	p	c
Coefficient	11.61	4.15	41.33
p-value	<0.0001	0.066	<0.0001
R²		0.901	

Table S6. Coefficient and p-value of parameters obtained from multiple linear regression of δ_{TBPO} with inclusion of β and π^* .

	b	p	c
Coefficient	-3.79	10.50	43.55
p-value	0.65	0.13	<0.0001
R²		0.148	

Table S7. Coefficient and p-value of parameters obtained from linear regression of δ_{TBPO} with α .

	a	c
Coefficient	12.08	44.13
p-value	<0.0001	<0.0001
R²	0.875	

Table S8. Coefficient and p-value of parameters obtained from linear regression of δ_{TBPO} with β .

	b	c
Coefficient	1.18	49.29
p-value	0.88	<0.0001
R²		0.002

Table S9. Coefficient and p-value of parameters obtained from linear regression of δ_{TBPO} with π^* .

	p	c
Coefficient	9.23	43.03
p-value	0.14	<0.0001
R²		0.135

Tables S3-S9 highlight that, as expected given the propensity of TBPO to act as a hydrogen bond acceptor, the α parameter has the greatest influence over the ^{31}P chemical shift of TBPO as its p-value was less than 0.0001 regardless of the number of other parameters present. Based on the data above, it appears that the model containing just α would be the most suitable. However, on examination of the data this model does not appear physically reasonable given the diversity of δ values obtained for solvents where $\alpha = 0$. Hence the model containing both α and π^* which yielded a good fit and statistical significance of the π^* coefficient at the 0.10 level, even if not at the 0.05 level of significance. This model is given by Equation S12 below.

$$\delta_{TBPO} = 11.606\alpha + 4.154\pi^* + 41.331 \quad (\text{S12})$$

Nile Red

The lowest energy absorption of Nile Red can be converted into an $E_T(\text{NR})$ value analogous to Reichardt's Dye 30 and 33 multiplying the inverse of the wavelength in nm by 28591.¹³ The calculation of the Kamlet-Taft parameter α from the Nile Red absorption spectrum has been determined empirically to be given by Equation S13 below, where $\bar{\nu}$ is the experimental wave number (cm^{-1}) of the lowest energy absorption maximum.¹⁴

$$\alpha = \frac{19.9657 - 1.0241\pi^* - \bar{\nu}_{NR}}{1.6078} \quad (\text{S13})$$

Polarity Parameter Results

Kamlet-Taft Parameters

Table S10 details the Kamlet-Taft parameters obtained for all of the DESs at each temperature. These results highlight that the apparent polarity of these solvents, as determined by the solvatochromic dye or pyridine N-oxide measurements, does not vary significantly with temperature as most changes in the observed parameters were less than ± 0.1 even on heating from 25 to 80°C which lies within the anticipated experimental error for these measurements. There is a slight decrease in observed α value with heating for many of the DES which is more clearly depicted by Figure S4 for selected DES compositions which may indicate weakening of the hydrogen bond network with increasing thermal energy; however, such an effect is clearly less than the effect of changing the identity of the DES itself.

Table S10. Kamlet-Taft parameters obtained for all DES at temperatures from 25-80°C. Parameters are defined in the text.

DES	GuCl:HBD	Temp (°C)	α_{RD}	α_{PyO}	α_{24}	α_{34}	β	π^*
GuCl:Gly	1:9	25	1.00	1.34	1.18	1.08	0.50	1.18
		40	0.95	1.31	1.15	1.06	0.44	1.22
		60	0.87	1.28	1.13	1.03	0.47	1.21
		80	0.86	1.24	1.09	1.00	0.44	1.21
	1:4	25	0.97	1.33	1.17	1.07	0.43	1.26
		40	0.92	1.31	1.15	1.05	0.44	1.27
		60	0.86	1.27	1.12	1.03	0.40	1.28
		80	0.86	1.24	1.09	1.00	0.44	1.24
	3:7	25	1.00	1.31	1.15	1.06	0.43	1.27
		40	0.93	1.28	1.13	1.04	0.40	1.30
		60	0.97	1.25	1.10	1.01	0.43	1.27
		80	0.93	1.22	1.07	0.99	0.39	1.27
	2:3	25	0.97	1.28	1.13	1.05	0.43	1.28
		40	0.92	1.26	1.11	1.03	0.38	1.30
		60	0.91	1.24	1.09	1.00	0.37	1.30
		80	0.89	1.20	1.06	0.98	0.36	1.29
Gly	-	25	0.91	1.34	1.18	1.06	0.53	1.14
		40	0.91	1.30	1.14	1.06	0.48	1.15
		60	0.86	1.26	1.11	1.03	0.49	1.14

		80	0.83	1.22	1.07	1.00	0.49	1.14
GuCl:LA	1:9	25		2.06	1.81	1.74	0.42	1.17
		40		2.05	1.80	1.73	0.40	1.19
		60		2.01	1.77	1.72	0.39	1.17
		80		2.00	1.76	1.70	0.35	1.17
	1:4	25		2.01	1.77	1.70	0.40	1.23
		40		2.01	1.77	1.69	0.35	1.25
		60		1.99	1.75	1.68	0.37	1.21
		80		1.97	1.73	1.67	0.38	1.18
	3:7	25		2.07	1.82	1.70	0.39	1.25
		40		2.07	1.82	1.70	0.39	1.25
		60		2.07	1.82	1.69	0.29	1.30
		80		2.06	1.81	1.68	0.31	1.27
	2:3	25		1.98	1.74	1.65	0.35	1.30
		40		1.98	1.74	1.65	0.33	1.33
		60		1.97	1.73	1.64	0.34	1.30
		80		1.95	1.72	1.63	0.36	1.23
LA	-	25		1.79	1.58	1.56	0.38	1.15
		40		1.76	1.55	1.54	0.41	1.11
		60		1.73	1.53	1.51	0.36	1.09
		80		1.70	1.50	1.48	0.31	1.09
GuCl:Acet	3:7	25	0.86	1.00	0.88	0.81	0.52	1.17
		40	0.90	1.00	0.88	0.81	0.54	1.14
		60	0.86	0.95	0.84	0.77	0.48	1.15
		80	0.86	0.92	0.81	0.75	0.52	1.11
	2:3	25	-	1.01	0.89	0.83	-	1.20
		40	0.88	0.83	0.73	0.81	0.49	1.21
		60	0.91	0.99	0.87	0.81	0.49	1.18
		80	0.85	0.97	0.85	0.79	0.47	1.17
GuCl:LevA	1:9	25		1.60	1.41	1.37	0.57	0.96
		40		1.58	1.39	1.35	0.53	0.98
		60		1.55	1.36	1.32	0.53	0.97
		80		1.51	1.33	1.30	0.54	0.91
	1:4	25		1.66	1.46	1.39	0.43	1.06
		40		1.64	1.44	1.38	0.46	1.04
		60		1.63	1.43	1.36	0.46	1.00
		80		1.60	1.41	1.34	0.47	0.96
LevA	-	25		1.49	1.31	1.31	0.96	0.58
		40		1.45	1.28	1.29	0.97	0.56
		60		1.41	1.24	1.26	0.98	0.53
		80		1.27	1.20	1.22	0.99	0.50

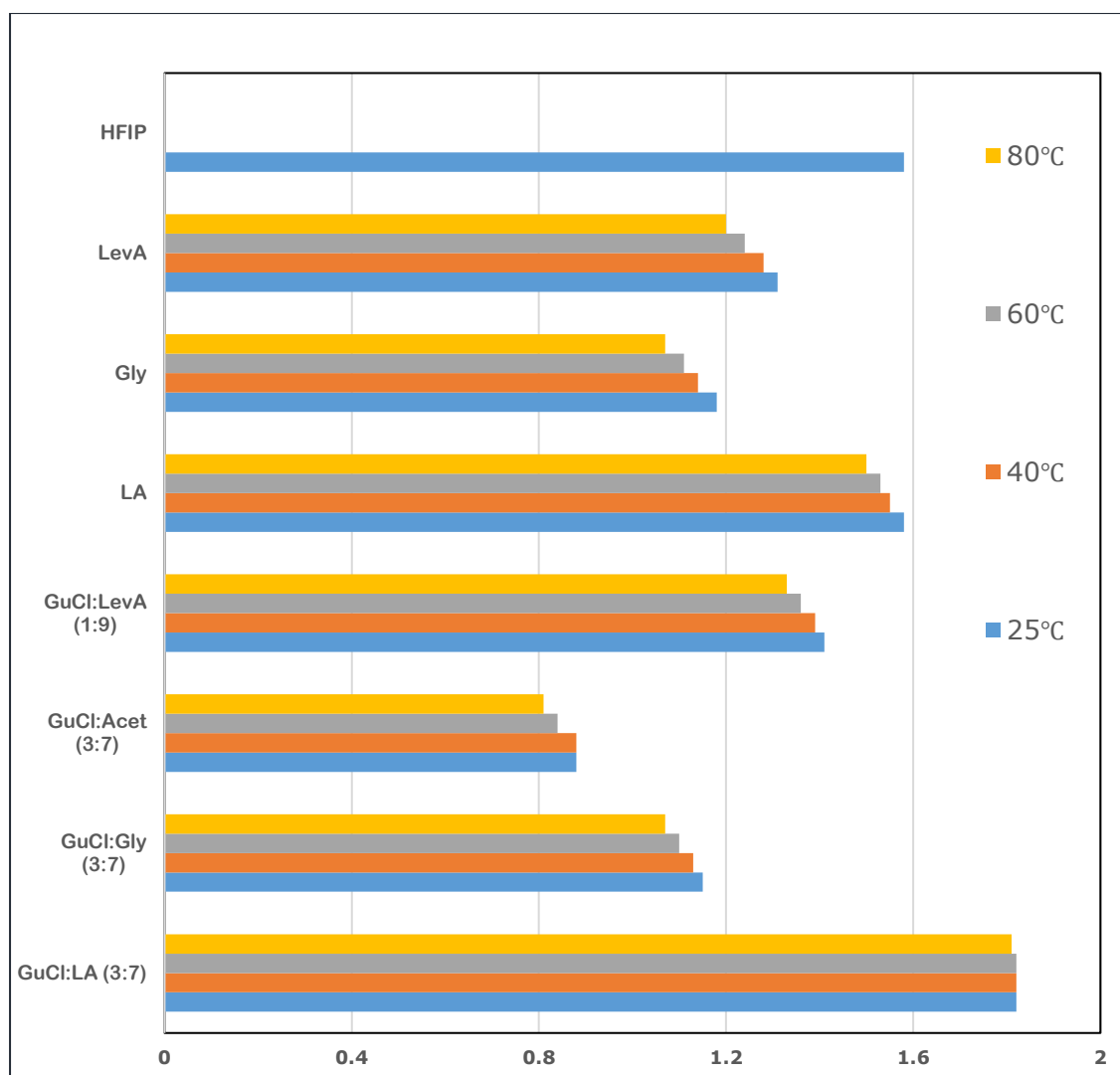


Figure S4. Effect of temperature on the α_{24} parameter for the DES

Nile Red Polarity Measurements

The Nile Red measurements are summarised in Table S11 including calculated $E_T(\text{NR})$ and α_{NR} values. As discussed in the paper, solvents containing LA and LevA led to a bifurcated Nile Red peak which is depicted in Figure S6. Gly containing solvents gave the anticipated peak shape depicted in Figure S5. The similar absorption spectra and bifurcated peak shapes for the LA and LevA solvents suggest that the Nile Red undergoes either a reaction or aggregation within these systems which limits its usefulness as a solvatochromic probe. This is highlighted by the large range of apparent $E_T(\text{NR})$ and α_{NR} values given in Table S11. These values are provided only for indicative purposes and are unlikely to represent genuine estimates of solvent polarity given the underlying chemical phenomena.

Table S11. Nile Red lowest energy absorption maxima, $E_T(\text{NR})$ and α_{NR} determined for the DES. Ranges were provided for the bifurcated peaks to highlight the span.

Solvent	GuCl:HBD	λ_{max} (nm)	$E_T(\text{NR})$	α_{NR}
Gly	-	580.6	49.24	0.98
GuCl:Gly	1:2	586.9	48.72	1.01
LA	-	639.6, 597.8*	44.70-47.83	1.28-1.96
GuCl:LA	1:2	639.6, 594.8*	44.70-48.07	1.17-1.90
GuCl:LevA	1:9	640.4, 596.5*	44.65-47.93	1.38-2.09

*Bifurcated peak (see Figure S6).

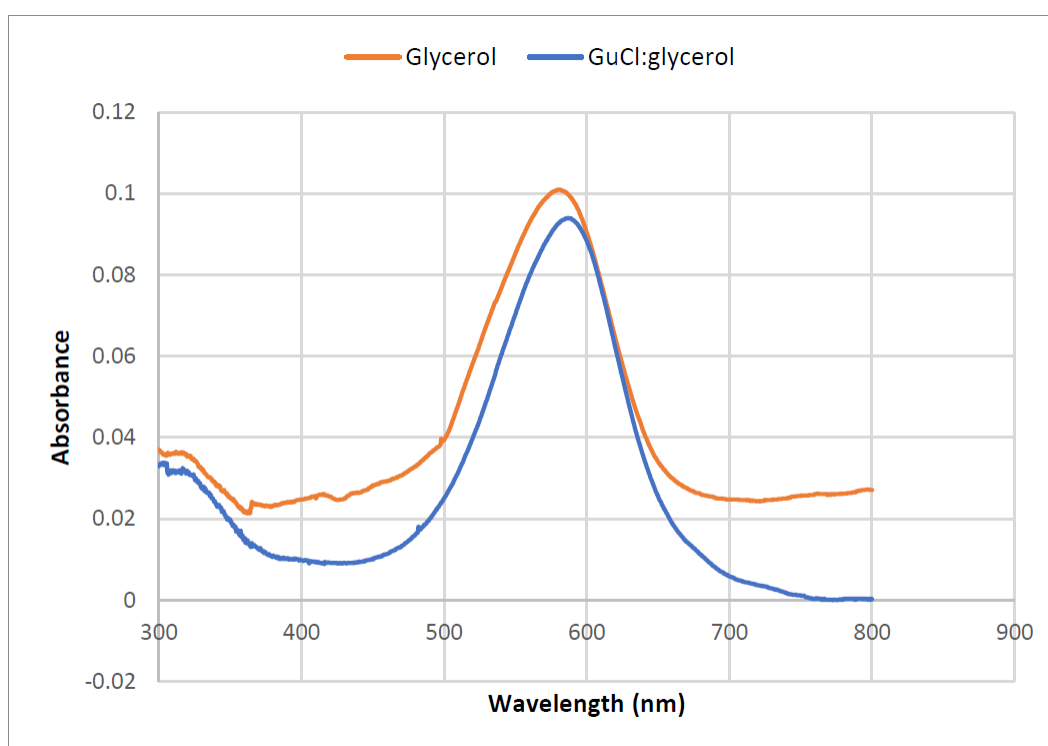


Figure S5. Nile Red UV-vis absorption spectrum for Gly and GuCl:Gly solvents.

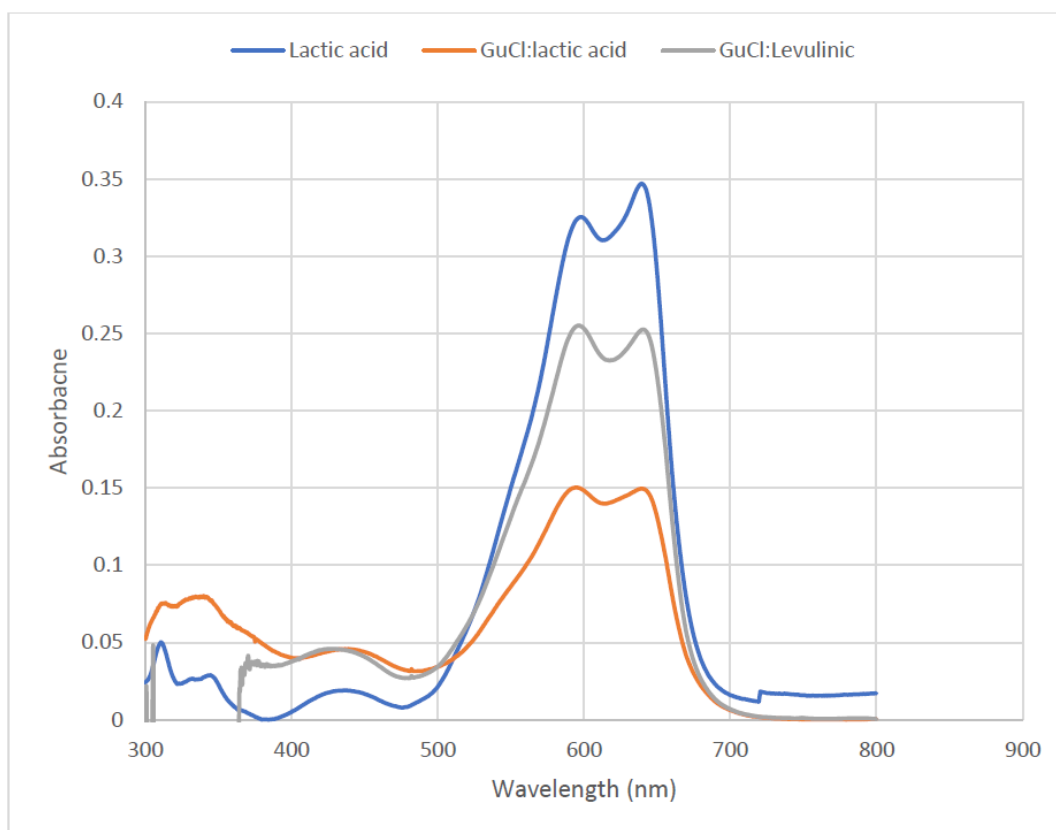


Figure S6. Nile Red UV-vis absorption spectrum for LA, GuCl:LA and GuCl:LevA solvents.

Density and Viscosity Measurements

The densities and viscosities of the DES at 20, 25, 40, 60 and 80°C are provided in Table S12. The viscosity measurements were made using the rolling ball method on an Anton Paar Lovis 2000 ME featuring a capillary with a 2.5 mm internal diameter. The experimental setup did not permit the measurement of viscosities less than 20 mPa s, hence solvents with a viscosity less than this are simply listed as < 20 mPa s in Table S12.

Table S12. Density and viscosity of DES at variable temperatures. Accuracy of density measurements is $\pm 0.0001 \text{ g cm}^{-3}$ and of viscosity measurements is $\pm 0.5\%$.

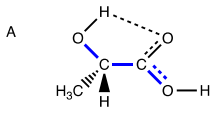
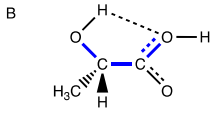
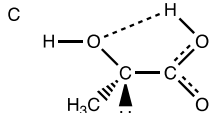
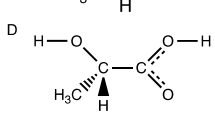
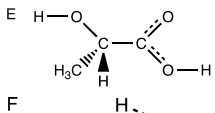
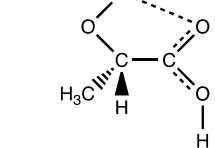
DES	GuCl:HBD	Temp (°C)	Density (g cm^{-3})	Viscosity (mPa s)
GuCl:LA	1:2	20	1.2472	181.4
		25	1.2436	126.8
		40	1.2331	50.05
		60	1.2193	20.60
		80	1.2054	<20

GuCl:Gly	1:2	20	1.2768	635.8
		25	1.2740	411.9
		40	1.2655	253.4
		60	1.2543	46.45
		80	1.2431	22.18
GuCl:LevA	1:9	20	1.1605	84.32
		25	1.1564	61.18
		40	1.1443	<20
		60	1.1276	<20
		80	1.1118	<20

Computational Details

The chemical species present can take on a range of stable conformers. LA has 6 stable isomers, ignoring the optical isomers which cannot be differentiated at this level of computation (due to the sub 1 kJ/mol energy difference), Table S13. The B3LYP/6-311+G(d,p) structures and energies compare favourably to those evaluated at the B3LYP-D3/aug-cc-pVTZ level.¹⁵ In a liquid environment dimers are also likely, Figure S7.

Table S13: Lactic acid conformers, ΔG in the gas-phase and ΔG in SMD-lactic-acid solvent and compared to ΔG from the literature evaluated at the B3LYP-D3/aug-cc-pVTZ level in the gas-phase.¹⁵ in kJ/mol.

Structure	ΔG gas-phase	ΔG lit gas-phase	ΔG lactic-acid
	0.0	0.0	0.0
	7.6	9.3	4.5
	10.2	9.9	3.6
	17.7	17.4	
	18.6	18.6	
	22.0	19.3	

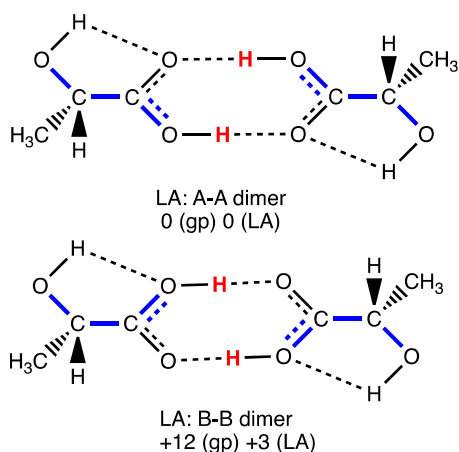


Figure S7. Lactic acid AA and BB dimers

The ionic salt ion-pair GuCl has two unique conformers, **A** with the Cl⁻ positioned between the NH₂ H-atoms and H-bonding to both, and **B** with the Cl⁻ undertaking an anion- π^+ interaction, Figure S8. Due to the symmetry of the Gu⁺ cation, there are three identical **A** conformers and two identical **B** conformers. The proton interacting with Cl⁻ is denoted as bridging (H_b) and the remainder are terminal (H_t).

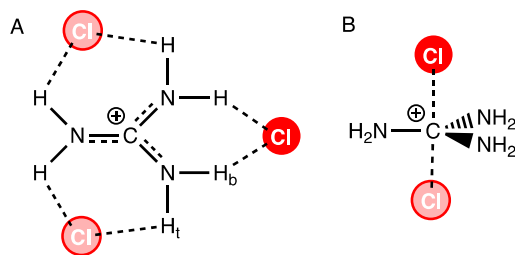


Figure S8: Conformers of GuCl

A qualitative estimate of the Kamlet-Taft α (α_{KT}) has been obtained employing the computed electrostatic potential (EP_{nuc}) at the most acidic H-atom, evaluated at B3LYP/6-311+G(d,p) level.⁴ The IL based empirical formula employed is $\alpha_{EP-IL}=5.153*EP_{nuc} + 5.136$. Alternatively an empirical relationship has also been determined by Platts for traditional (neutral) molecular solvents at the HF/6-31G(d)//B3LYP/6-311G(d,p) level for the Abrahams α $\alpha_{AB}=\sum\alpha_H^{2.16}$ $\alpha_{AB}=6.102*EP_{nuc} + 6.562$. We have converted the Abrahams alpha to the KT alpha using $\alpha_{AB}=0.4098\alpha_{KT} + 0.0064$.⁶ Thus, $\alpha_{EP-NE}=14.890*EP_{nuc} + 15.997$. Here we use data evaluated at the B3LYP/6-311+G(d,p) level to determine the "Platts" values.

Initially, α_{EP} has been evaluated for representative species using the ionic and neutral methodologies, and has been compared to the experimental data evaluated via α_{RD} or through α_{24} , Table S14. The probe molecule must act in competition with other H-bonding acceptors,

moreover each molecule will be affected by interactions with other molecules in the first solvation sphere, **Figure S9**. Pure LA has been evaluated for conformer **A** and the dimer **AA**, LA has $\alpha_{EP} \approx 2.0$, which is comparable to α_{EP} evaluated for HFIP, but consistent with the high α_{RD}/α_{24} evaluated for both LA and HFIP. The values for α_{EP} are a little high and thus provide qualitative rather than quantitative information.

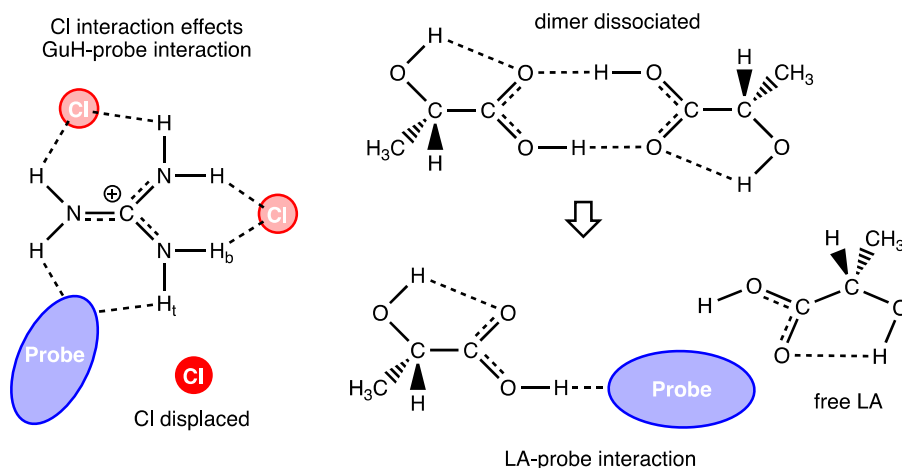


Figure S9: Conformers of GuCl

Table S14. Computational and experimental "Kamlet Taft" α values. HFIP is 1,1,1,3,3,3-hexafluoro-2-propanol. $[\text{C}_4\text{C}_1\text{im}]^+$ is the 1-butyl-3-methylimidazolium cation.

H-atom	EP_{nuc}	$\alpha_{\text{EP-IL}}$ (ionic liquid)	$\alpha_{\text{EP-NE}}$ (neutral)	$\alpha_{\text{RD}}/\alpha_{24}$ (exp.)
HFIP	-0.945	0.27	1.93	1.58
LA monomer-A	-0.935	0.32	2.08	1.58
LA-dimer AA	-0.939	0.29	2.01	1.58
$[\text{C}_4\text{C}_1\text{im}]^+$	-0.873	0.64	2.99	0.63-0.77 ⁹
$[\text{C}_4\text{C}_1\text{im}][\text{BF}_4]$	-1.025	-0.12	0.80	0.63-0.77 ⁹
Gu^+	-0.801	1.01	4.07	-
GuCl	-0.953	0.22	1.81	-

In an IL with a weakly coordinating anion the cation is essentially isolated within a generalised solvation environment and $\alpha_{\text{EP-IL}}$ provides the best computational estimate, as is shown for $[\text{C}_4\text{C}_1\text{im}]^+$. With the counter-ion explicitly present the ion-pair is neutral and $\alpha_{\text{EP-NE}}$ is a better estimate. Computationally $\alpha_{\text{EP-IL}}$ and $\alpha_{\text{EP-NE}}$ can be considered as estimates for the extremes of interactions occurring within the IL. Pure GuCl is a solid and $\alpha_{\text{RD}}/\alpha_{24}$ cannot be experimentally measured; however, computationally $\alpha_{\text{EP-IL}}$ has been estimated for Gu^+ and $\alpha_{\text{EP-NE}}$ for the ion-pair GuCl giving a range of α_{EP} from 1.01-1.81 which is significantly higher than the α_{EP} determined for $[\text{C}_4\text{C}_1\text{im}]^+$ and comparable to the high values determined both computationally and experimentally for pure LA and HFIP.

Experimentally the addition of 10% GuCl raises the measured α_{24} from 1.58 to 1.81, an increase of 0.23 or 15%. With the reference values for the pure components, a computational estimate for α_{EP} has been determined for the GuCl:LA mixture, Table S15. The computational data indicate GuCl ($\alpha_{EP} \approx 1$) will not raise the H-bonding ability of a predominantly LA ($\alpha_{EP} \approx 2$) mixture though simple addition. The increase in α_{24} is therefore indicative of a cooperative H-bonding and/or selective solvation effect.

In DESs the reduction in melting point is often associated with the reduction in Coulomb interactions due to HBD interaction with the anion, in this case LA coordination of the Cl^- anion. More recently the importance of cation-HBD interactions has been identified.¹⁷ Thus the pair-wise interactions of $[\text{Gu-LA}]^+$ and $[\text{Cl-LA}]^-$ have been investigated. We note that an exhaustive conformational search has not been carried out, but reasonable H-bonded (low energy) conformers have been examined.

Cl^- conformers were formed and optimised that maximised the H-bonding with LA-A or LA-B, Figure S10a. The lowest energy (gas phase) structure is cyclic with Cl interacting with both the COOH and OH protons of LA-A. However, in the solvent phase a linear structure with a larger overall charge arm (the ion equivalent of a dipole) is slightly favoured; the Cl interacts with just the COOH of LA-B. In both conformers the COOH H-atom is engaged in H-bonding with the Cl^- and thus the α_{EP} drops significantly. Thus, interaction of the LA with Cl^- does not directly lead to an increase in α .

$[\text{Gu-LA}]^+$ conformers were formed with LA-A/B with the carboxylic oxygen interacting with the Gu^+ protons. The more stable conformer has (higher energy) LA-B forming an interaction through just one O-atom, just slightly higher in energy is a LA-A conformer forming a more complex array of H-bonds with both the OH and COOH O-atoms, Figure S10b. In both conformers the COOH H-atom (LA) and terminal NH_2 H-atom (Gu) are available however a small drop in α_{EP} is determined. Thus, interaction of the LA with Gu^+ does not directly lead to an increase in α .

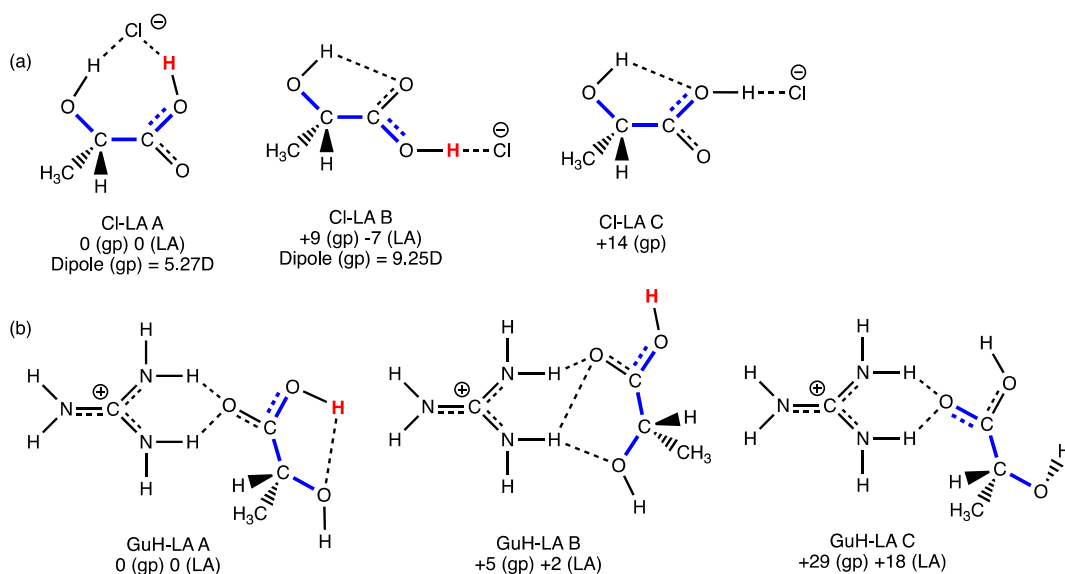


Figure S10. Conformers for the pair-interactions, blue dihedrals indicate LA-A (trans) or LA-B (cis) and red protons indicate those with the lowest EP_{nuc}

Table S15. NBO charge, EP_{nuc} and α_{EP} for the relevant H atoms of each molecule.

	H-atom	NBO	EP_{nuc}	α_{EP}
LA (isolated)	A-COOH	+0.49	-0.935	2.08
	A-OH	+0.48	-0.998	1.14
	B-COOH	+0.49	-0.937	2.03
	B-OH	+0.47	-0.991	1.23
LA (dimers)	AA-COOH	+0.49	-0.935	2.08
	BB-COOH	+0.51	-0.938	2.03
Gu ⁺	-H _t	+0.43	-0.801	1.01
GuCl	-H _b	+0.44	-0.993	1.22
	-H _t	+0.40	-0.953	1.81
[Cl-LA] ⁻	cyclic LA-A COOH	+0.50	-1.119	-0.63
	linear LA-B COOH	+0.48	-1.119	-0.63
[Gu-LA] ⁺	confA-COOH LA-A	+0.51	-0.835	0.83
	confA-GuH _t	+0.41	-0.840	0.81
	confB-COOH LA-B	+0.50	-0.823	0.89
	confB-GuH _t	+0.42	-0.840	0.81
GuCl•LA	cyclic-Gu-H _t	+0.40	-0.949	1.87
	cyclic-Gu-H _b (LA)	+0.47	-0.981	1.38
	cyclic-Gu-H _b (Cl)	+0.43	-0.989	1.26
	cyclic-LA COOH	+0.49	-0.981	1.39
	cyclic-LA OH	+0.48	-1.015	0.89
	linear-Gu-H _t	+0.39	-0.973	1.51
	linear-Gu-H _b (LA)	+0.42	-0.978	1.43
	linear-Gu-H _b (Cl)	+0.44	-1.009	0.97
	linear-LA COOH	+0.50	-0.901	2.58
	linear-LA OH	+0.48	-0.964	1.65

The molecular effect of introducing GuCl to LA can be probed by considering a 1:1 cluster GuCl•LA. A change in H-bond donating ability of a mixture could be due to an increase in the ability of the LA COOH to donate, or the ability of the Gu NH₂ to donate. GuCl•LA clusters can form with a "cyclic" structure where LA is interacting with both Cl and Gu and a slightly higher energy "linear" form with LA where the COOH remains available for interaction with a probe molecule, Figure S11. The linear-GuCl•LA has a *significantly enhanced* $\alpha_{EP}=2.58$ (relative to 2.08) and cyclic-GuCl•LA has a slightly elevated GuH-H_t $\alpha_{EP}=1.87$ (relative to 1.81).

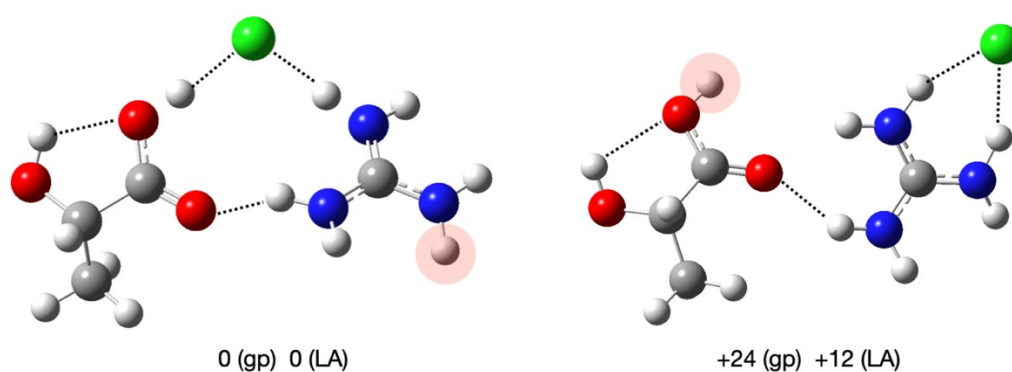


Figure S11: GuCl•LA clusters, areas shaded red are the enhanced COOH and GuH-H_t reported in Table S15

While a small amount of GuCl is sufficient to lift the H-bond donating ability of the mixture, the maximum miscibility of GuCl in LA is reached just beyond a ratio of GuCl at 1:2 (GuCl:LA). Beyond this point the GuCl precipitates out.

When GuCl is added to the LA, it is anticipated that dissolution of the solid crystal into individual ion-pairs that are solvated by LA occurs. The Gibbs free energy for the breakup of any LA•LA dimers is minimal $\Delta G=+7$ kJ/mol. The generalised solvation Gibbs free energy of GuCl in LA is $\Delta G_{\text{solv}}=-79$ kJ/mol. Once the ion-pair is solvated, further dissociation into the individual ions $\text{Gu}^+ + \text{Cl}^-$ is not favoured within LA, $\Delta G\approx+63$ kJ/mol.

The Gibbs free energy for direct association of LA with the ion-pair ($\text{GuCl} + \text{LA} \rightarrow \text{GuCl}\cdot\text{LA}$) is $\Delta G\approx+4$ kJ/mol. Direct association of another LA is also possible room temperature, $\Delta G\approx+7$ kJ/mol. Direct association with to form $[\text{Gu}\cdot\text{LA}]^+$ is $\Delta G=0$ kJ/mol, while association to form $[\text{Cl}\cdot\text{LA}]^-$ is slightly favoured $\Delta G=-14$ kJ/mol. Once the LA associated ions are formed; $[\text{GuH}\cdot\text{LA}]^+$ and $[\text{Cl}\cdot\text{LA}]^-$ easily combine to form the cluster $\text{GuCl}\cdot\text{LA}_2$ $\Delta G=-46$ kJ/mol. Thus, we have established that the dissolution of GuCl and formation of $\text{GuCl}\cdot\text{LA}$ or $\text{GuCl}\cdot\text{LA}_2$ in bulk LA is favourable. The formation of the $\text{GuCl}\cdot\text{LA}$ cluster leading to the high α_{EP} value is favourable. The Gibbs free energies of these processes are summarised in Table S16.

Table S16. Association energies (E_{ass}) and Gibbs free energies (G_{ass}) in kJ/mol for cluster components.

	E_{ass}	G_{ass}	G_{ass}
	gp	gp	SMD-LA
$\text{GuCl} \rightarrow \text{Gu}^+ + \text{Cl}^-$	+455	+434	+63
$(\text{LA})_2 \rightarrow 2\text{LA}$	+66	+15	+7
$\text{Cl}^- + \text{LA} \rightarrow [\text{Cl}\cdot\text{LA}]^-$	-119	-87	-14
$\text{Gu}^+ + \text{LA} \rightarrow [\text{Gu}\cdot\text{LA}]^+$	-91	-54	0
$[\text{Cl}\cdot\text{LA}]^- + \text{LA} \rightarrow [\text{LA}\cdot\text{Cl}\cdot\text{LA}]^-$	-69	-32	-1
$\text{GuCl} + \text{LA} \rightarrow \text{GuCl}\cdot\text{LA}$	-56	-10	+4
$\text{GuCl}\cdot\text{LA} + \text{LA} \rightarrow \text{GuCl}\cdot\text{LA}_2$	-46	+13	+7
$\text{Gu}^+ + [\text{Cl}\cdot\text{LA}]^- \rightarrow \text{GuCl}\cdot\text{LA}$	-392	-357	-53
$[\text{Cl}\cdot\text{LA}]^- + [\text{Gu}\cdot\text{LA}]^+ \rightarrow \text{GuCl}\cdot\text{LA}_2$	-348	-291	-46
$[\text{LA}\cdot\text{Cl}\cdot\text{LA}]^- + \text{Gu}^+ \rightarrow \text{GuCl}\cdot\text{LA}_2$	-345	-302	-38
$\text{GuCl} + (\text{LA})_2 \rightarrow \text{GuCl}\cdot\text{LA}_2$	-37	+18	+21

Each Gu^+ has three primary H-bonding sites, Figure S12a. In a solvated ion-pair Cl^- occupies one position, and LA the other two. If the ratio of LA drops, a second Cl^- (with a corresponding Gu^+) can occupy a H-bonding site, initiating the formation of an ionic domain. Thus, at mole ratios above 1:2 we can rationalise the precipitation of GuCl .

The experimental data suggests a ratio of $\text{GuCl}:\text{LA}$ of 1:2 is of interest. The changing number and type of H-bonds increasing the possible H-bonding configurations (ie the entropy of the liquid) is thought to be a key driver in IL based DES formation. If the quantity of GuCl in LA is dilute, we can imagine a mixture primarily of LA-LA H-bonds with only a few of the "new" Gu-LA and Cl-LA H-bonds. As the amount of GuCl increases the distribution and ways of arranging H-bonds significantly increases.

Anion- π interactions as well as $\pi^+ - \pi^+$ interactions are possible within this system, and have been observed for the pure GuCl and for the LA interacting with the Gu^+ cation, Figure S12b.

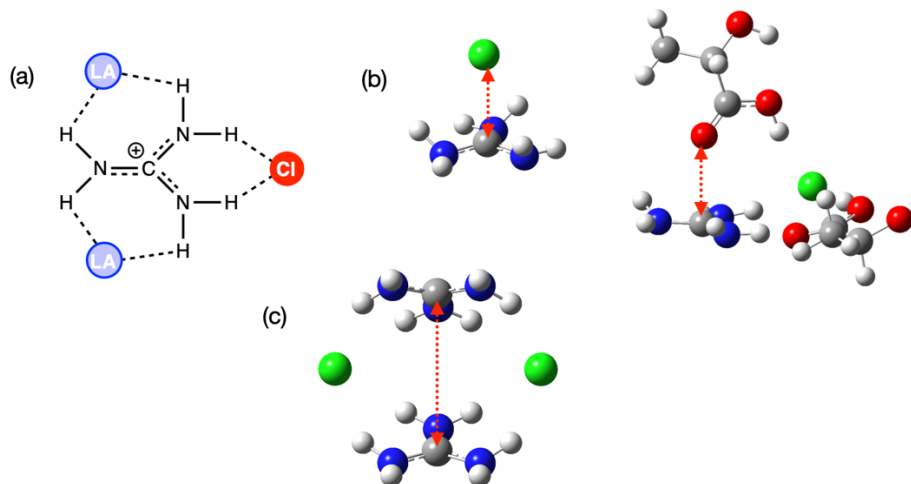


Figure S12: (a) 1:2 ratio of GuCl:LA, (b) Anion- π^+ and (c) π^+ - π^+ interactions.

References

1. N. J. Brooks, F. Castiglione, C. Doherty, A. Dolan, A. J. Hill, P. A. Hunt, R. P. Matthews, M. Mauri, A. Mele, R. Simonutti, I. J. Villar-Garcia, C. C. Weber and T. Welton, *Chem. Sci.*, 2017, **8**, 6359-6374.
2. A. Brandt, J. P. Hallett, D. J. Leak, R. J. Murphy and T. Welton, *Green Chem.*, 2010, **12**, 672-679.
3. P. P. Madeira, H. Passos, J. Gomes, J. A. P. Coutinho and M. G. Freire, *Phys. Chem. Chem. Phys.*, 2017, **19**, 11011-11016.
4. H. Niedermeyer, C. Ashworth, A. Brandt, T. Welton and P. A. Hunt, *Phys Chem Chem Phys*, 2013, **15**, 11566-11578.
5. A. V. Marenich, C. J. Cramer and D. G. Truhlar, *The Journal of Physical Chemistry B*, 2009, **113**, 6378-6396.
6. V. S. Bernales, A. V. Marenich, R. Contreras, C. J. Cramer and D. G. Truhlar, *J Phys Chem B*, 2012, **116**, 9122-9129.
7. C. Dichtl, P. Sippel and S. Krohns, *Advances in Materials Science and Engineering*, 2017, **2017**, 1-10.
8. J. R. Rumble, ed., *CRC Handbook of Chemistry and Physics*, CRC Press, Taylor & Francis Group, 2021.
9. M. A. Ab Rani, A. Brant, L. Crowhurst, A. Dolan, M. Lui, N. H. Hassan, J. P. Hallett, P. A. Hunt, H. Niedermeyer, J. M. Perez-Arlandis, M. Schrems, T. Welton and R. Wilding, *Phys. Chem. Chem. Phys.*, 2011, **13**, 16831-16840.
10. C. Florindo, A. J. S. McIntosh, T. Welton, L. C. Branco and I. M. Marrucho, *Phys. Chem. Chem. Phys.*, 2018, **20**, 206-213.
11. C. Reichardt and T. Welton, *Solvents and Solvent Effects in Organic Chemistry*, Wiley-VCH Verlag & Co. KGaA, Weinheim, 4th edn., 2011.
12. R. Stenutz, Kamlet-Taft solvent parameters, <http://www.stenutz.eu/chem/solv26.php>, 2020).
13. J. F. Deye, T. A. Berger and A. G. Anderson, *Anal. Chem.*, 1990, **62**, 615-622.
14. A. K. Dwamena and D. E. Raynie, *J. Chem. Eng. Data*, 2020, **65**, 640-646.
15. C. D. Zeinalipour-Yazdi and C. R. A. Catlow, *Phys Chem Chem Phys*, 2019, **21**, 22331-22343.
16. J. A. Platts, *Phys. Chem. Chem. Phys.*, 2000, **2**, 973-980.
17. C. R. Ashworth, R. P. Matthews, T. Welton and P. A. Hunt, *Phys Chem Chem Phys*, 2016, **18**, 18145-18160.